Calculations for ambient dose equivalent rates in nine forests in eastern Japan from ^{134}Cs and ^{137}Cs radioactivity measurements

Alex Malins[1*], Naohiro Imamura[2], Tadafumi Niizato[3], Junko Takahashi[4], Minsik Kim[1], Kazuyuki Sakuma[3], Yoshiki Shinomiya[2], Satoru Miura[2], Masahiko Machida[1]

[1] Japan Atomic Energy Agency, Center for Computational Science and e-Systems, 178-4-4 Wakashiba, Kashiwa, Chiba 277-0871, Japan

[2] Forestry and Forest Products Research Institute, 1 Matsunosato, Tsukuba, Ibaraki 305-8687, Japan

[3] Japan Atomic Energy Agency, Collaborative Laboratories for Advanced Decommissioning Science (CLADS) Environmental Research Group, 10-2 Fukasaku, Miharu-machi, Tamura-gun, Fukushima 963-7700, Japan

[4] Center for Research in Isotopes and Environmental Dynamic, University of Tsukuba, Tennodai 1-1-1, Tsukuba-shi Ibaraki, 305-8572, Japan

[*]Corresponding author: malins.alex@jaea.go.jp

Highlights

- Monte Carlo simulations for $\dot{H}^*(10)$ in forests in Japan between 2011 and 2017 from ^{134}Cs and ^{137}Cs radioactivity measurements
- Mean residual error between simulated $\dot{H}^*(10)$ at 1 m and handheld survey meter measurements was 16%.
- Calculated the contributions from ^{134}Cs and ^{137}Cs located in different parts of the forests to $\dot{H}^*(10)$.
- Largest contributions were from ^{134}Cs and ^{137}Cs in the canopy, organic layer and top 5 cm of soil.
- Uncertainties were evaluated in simulation results based on measurement uncertainties in model inputs.

Abstract

Understanding the relationship between the distribution of radioactive ^{134}Cs and ^{137}Cs in forests and ambient dose equivalent rates ($\dot{H}^*(10)$) in the air is important for researching forests in eastern Japan affected by the Fukushima Dai-ichi Nuclear Power Plant (FDNPP) accident. This study used a large number of measurements from forest samples, including ^{134}Cs and ^{137}Cs radioactivity concentrations, densities and moisture contents, to perform Monte Carlo radiation transport simulations for $\dot{H}^*(10)$ between 2011 and 2017. Calculated $\dot{H}^*(10)$ at 0.1 and 1 m above the ground had mean residual errors of 19% and 16%, respectively, from measurements taken with handheld NaI(Tl) scintillator survey meters. Setting aside the contributions from natural background radiation, ^{134}Cs and ^{137}Cs in the organic layer and the top 5 cm of forest soil generally made the largest contributions to calculated $\dot{H}^*(10)$. The contributions from ^{134}Cs and ^{137}Cs in the forest canopy were calculated to be largest in the first two years following the accident. Uncertainties were evaluated in the simulation results due to the measurement uncertainties in the model inputs by assuming Gaussian measurement errors. The mean uncertainty (relative standard deviation) of the simulated $\dot{H}^*(10)$ at 1 m height was 11%. The main contributors to the total uncertainty in the simulation results were the accuracies to which the ^{134}Cs and ^{137}Cs radioactivities of the organic layer and top 5 cm of soil, and the vertical distribution of ^{134}Cs and ^{137}Cs within the 5 cm soil layers, were known. Radioactive cesium located in the top 5 cm of soil was the main contributor to $\dot{H}^*(10)$ at 1 m by 2016 or 2017 in the calculation results for all sites. Studies on the ^{137}Cs distribution within forest soil will therefore help explain radiation levels henceforth in forests affected by the FDNPP accident. The merits of this study are that it modelled multiple forests for a long time period, with the important model inputs being informed by field measurements, and it quantified how the measurement uncertainties in these inputs affected the calculation results.

54 Keywords: forests; ambient dose equivalent rate; simulation; Fukushima Dai-ichi Nuclear
55 Power Plant accident; Monte Carlo

1. Introduction

After the Fukushima Dai-ichi Nuclear Power Plant (FDNPP) accident in 2011, around 70% of the atmospheric ^{134}Cs and ^{137}Cs fallout in eastern Japan landed on forests (Hashimoto et al., 2012; Kato et al., 2019). The management of these forests is an important issue in affected regions as around 40% by area are plantations (Forestry Agency of Japan, 2012) and forestry products make an important contribution to local economies (Miura, 2016). It has been shown that ^{134}Cs and ^{137}Cs transfers slowly from forests to rivers (Evrard et al., 2015) and freshwater fish (Wada et al., 2019; Kurikami et al., 2019). Thus economic and environmental considerations need to be taken into account when evaluating future management choices for the forests.

Studies often utilize mathematical relationships that connect ambient radiation levels measured in the air with quantities of radioactive cesium for monitoring radioactivity levels in the environment (UNSCEAR, 2000; Sanada et al., 2014; Mikami et al., 2015a; Karadeniz et al., 2015; Sakuma et al., 2018a). The numerical parameters in these relationships are derived from radiation transport calculations (Beck et al., 1972; ICRU, 1994; Saito and Jacob, 1995; Saito and Petoussi-Henss, 2014). Calculations applicable for forests were first performed for sites affected by atmospheric nuclear weapons test and Chernobyl accident fallout (Miller et al., 1990; Clouvas et al., 1999; Golikov et al., 1999; Gering et al., 2002; Clouvas et al., 2005). The relationship between ^{134}Cs and ^{137}Cs radioactivities in forests affected by the FDNPP accident and radiation levels in the air has been modelled with various methodologies. These include using simple analytical expressions for attenuation (Imamura et al., 2017a), or by interpolating published ^{134}Cs and ^{137}Cs radioactivity to ambient dose equivalent rate conversion coefficients to model forest soil layers and the organic layer (Teramage and Sun; 2020). More comprehensive assessments have employed Monte Carlo radiation transport simulations (Gonze et al., 2016; Hemmi, 2017; Cresswell et al., 2018: Sakuma et al., 2018b).

Radiation transport models of forests are necessarily more complex than models for open sites, such as farmland and recreational spaces, as they need to account for the radioactivity present in trees and the forest organic layer, and the shielding of gamma rays within these parts of forests. The radioactivity distribution in forests also changes dynamically over time due the forest ecosystem (Hashimoto et al., 2020). Required input data for forest radiation transport models include physical dimensions of trees, ^{134}Cs and ^{137}Cs radioactivity distributions, and densities and moisture contents of different materials in forests. The large number of inputs required mean that it is unusual for a single published forest measurement survey to contain all necessary data for creating a realistic radiation transport model of a forest.

This study modelled ambient dose equivalent rates ($\dot{H}^*(10)$) to high accuracy in nine forests in eastern Japan for a long time period (2011–17) by collating measurements from multiple field surveys to set up the models. The various measurements were used to simulate $\dot{H}^*(10)$ at 0.1, 1 and 20 m above the ground using the Monte Carlo radiation transport method. In addition to the main calculations for $\dot{H}^*(10)$, this paper presents the following: (i) verification of the simulated $\dot{H}^*(10)$ by comparing against measurements taken with handheld NaI(Tl) scintillator survey meters in the forests; (ii) calculations of the separate contributions to $\dot{H}^*(10)$ from ^{134}Cs and ^{137}Cs located within the canopy, tree trunks, the forest organic layer and different depth soil layers to determine the main sources of radioactivity contributing to $\dot{H}^*(10)$; and (iii) a Monte Carlo uncertainty analysis of the effects of measurement uncertainties in the model inputs on the simulation results. The merits of this study are that it modelled multiple forests for a long period following the FDNPP accident in 2011, and that all the major input parameters in the models were set based on survey data from forests in eastern Japan.

2. Methods

2.1 Surveys by Forestry and Forest Products Research Institute

Physical measurements and ^{134}Cs and ^{137}Cs distributions for nine forests were surveyed by the Forestry and Forest Products Research Institute (FFPRI) and the Forestry Agency of Japan between 2011 and 2017 (Imamura et al., 2017b; Forestry Agency of Japan, 2017; 2018). Each forest was referenced by a code denoting the forest location and the dominant species of trees. The forests were located in the Kawauchi (location code KU), Otama (OT), and Tadami (TD) districts in Fukushima Prefecture, and the Ishioka (*Tsukuba* – TB) district in Ibaraki Prefecture. The main tree species were evergreen coniferous trees of Japanese cedar (sugi, *Cryptomeria japonica* – species code S), Japanese cypress (hinoki, *Chamaecyparis obtusa* – H), Japanese red pine (akamatsu, *Pinus densiflora* – P) and deciduous broadleaf trees of konara oak (*Quercus serrata* – Q).

Site OT-S is a single species plantation of Japanese cedar (Table 1). Sites KU1-S and TD-S contain mainly Japanese cedars, but also include some deciduous broadleaf species trees with lower prevalence than Japanese cedar such as konara oak and deciduous Japanese chestnut (*Castanea crenata*). Site KU2-S contains Japanese cedars, with deciduous conifers of Japanese larch (karamatsu, *Larix kaempferi*) and other deciduous broadleaf species trees at lower prevalence. Sites KU-H and TB-H are single species plantations of Japanese cypress. Site KU1-Q is a secondary forest of konara oaks and other broadleaf species trees. Sites OT-P and OT-Q are secondary forests containing Japanese red pines and konara oaks plus other deciduous broadleaf species trees.

Research plots were established at each site with areas between 0.06 and 0.24 ha. Surveys were undertaken annually, usually in August or September, for the survey periods in Table 1. All measured ^{134}Cs and ^{137}Cs radioactivities in the samples were decay corrected to 1st September of the applicable sampling year.

2.1.1 Tree measurements

Stand counts and diameters at breast height (DBH) were taken for all trees (n = 4 to 268) within each species group at the research plots (Kajimoto et al., 2014). Tree heights (m) were estimated using DBH allometric equations applicable for each species group. The parameters in the DBH allometric equations were derived using a sample of tree heights of the main species trees measured using a laser rangefinder (Kajimoto et al., 2014).

Total oven-dried biomass quantities (kg/m^2) of leaves/needles, branches, bark, sapwood and heartwood for each species group were calculated using stand densities and DBH allometric equations. The parameters in DBH allometric equation were derived from samples taken from main species trees that were felled each year from 2011 to 2016 (Kajimoto et al., 2014; Komatsu et al., 2016). Trees (n = 3) with differing trunk diameters (small, medium and large) were felled each year during this period (Kuroda et al., 2013; Kajimoto et al., 2014). Wood disks were cut from the felled trunks and split into bark, sapwood and heartwood sections. For 2017, samples from trunks were taken by the tree ring core method at sites KU1-H, KU1-Q, KU1-S and KU2-S, while three trees were felled at site OT-Q as per the sampling methodology in earlier years. Branch and needle/leaf samples were taken for 2011 to 2017 (n = 3 to 4).

The samples were oven-dried, weighed and the ^{134}Cs and ^{137}Cs contents (Bq/kg) measured using gamma spectroscopy (n = 3 to 4) (Imamura et al., 2017b; Kenzo et al., 2020). Lowest live branch heights were measured on the sampled trunks (n = 3). Moisture contents (defined as the ratio of the water to oven-dried material mass) of the bark, sapwood and heartwood were calculated from the wood disk samples (n = 4 to 8) (Kuroda et al., 2013; Ohashi et al., 2017).

For forests with more than one group of tree species (sites KU1-S, KU2-S, OT-Q, OT-P and TD-S), data (including DBH equations) for the lower prevalence group(s) were inferred using data from another site where the corresponding species group was the main species group (Table S1). For example, data for Japanese red pines at site OT-Q were estimated using the Japanese red pine data from site OT-P. For the cases where it was necessary to infer data from

other sites, ^{134}Cs and ^{137}Cs radioactivities were scaled to account for any intrinsic differences in fallout radioactivity levels between the sites (Komatsu et al., 2016).

2.1.2 Forest organic layer and soil measurements

Samples of the organic layer were gathered from 25 × 25 cm quadrats on the forest floor (n = 6 to 12). Soil was sampled in 5 cm layers down to 20 cm depth using a metal core sampler (n = 3 to 12) (Fujii et al., 2014; Ikeda et al., 2014; Komatsu et al., 2016; Manaka et al., 2019). The samples were oven-dried, weighed and the ^{134}Cs and ^{137}Cs radioactivities measured using high purity gamma spectroscopy detectors. The results were used to calculate mean oven-dried densities (kg/m^3) and ^{134}Cs and ^{137}Cs inventories (Bq/m^2) of the organic layer and soil layers. Following Imamura et al. (2017a), the organic layer was assumed to be 4 cm thick for the calculations.

2.1.3 Measurement of ambient dose equivalent rates

Ambient dose equivalent rates at 0.1 and 1 m heights above the ground surface were measured using handheld NaI(Tl) scintillator survey meters (TCS-172B, Hitachi-Aloka Medical, Ltd., Tokyo, Japan). Measurements were taken at the vertices of 10 × 10 m grid squares within each plot (Ikeda et al., 2014; Imamura et at., 2015; Komatsu et al., 2016). The mean values of the measurements (n = 6 to 36) at each height were used for comparison with the simulation results.

2.2 Data from surveys of other forest sites

Not all measurements necessary for creating a radiation transport model to link the ^{134}Cs and ^{137}Cs radioactivity distribution in the forests with $\dot{H}^*(10)$ were available from the surveys by FFPRI. The moisture contents of the branches and needles/leaves of trees, the organic layer

and the soil layers were not measured during the FFPRI surveys, but these data are needed to model the overall densities and elemental compositions of these materials, which affect the attenuation of ^{134}Cs and ^{137}Cs gamma rays. The vertical distribution of ^{134}Cs and ^{137}Cs in soil was also only measured to the resolution of 5 cm thick soil layers in these surveys. In reality it is typical for the concentration of ^{134}Cs and ^{137}Cs in forest soils in eastern Japan to decrease exponentially with depth (Teramage et al., 2016; Yoschenko et al., 2017; Muto et al., 2019). Previous studies have reported a relaxation depth of the exponential function, α, on the order of 0.5 to 5 cm (Mishra et al., 2016; Takahashi et al., 2018). Thus it is necessary to model the vertical distribution of ^{134}Cs and ^{137}Cs in soil with a finer resolution than 5 cm thick soil layers for forest $\dot{H}^*(10)$ calculations. As outlined below, moisture contents for the canopy, organic layer and soil, and data on the vertical distribution of ^{134}Cs and ^{137}Cs within soil, were obtained from different forest surveys for set up the simulation models.

2.2.1 Moisture contents of branches and needles/leaves

Data for the moisture contents of branches and needles/leaves came from forest sites in the Kawamata and Kawauchi districts of Fukushima Prefecture monitored by Japan Atomic Energy Agency (JAEA) (Niizato et al., 2016). Needle and branch samples of Japanese cedars were taken from the upper, middle and lower parts of the crowns of five trees in the Kawauchi forest on 27–29 October 2015 and on 25–27 September 2017. The mean moisture contents of these samples were used to model the moisture contents of the needles and branches of the evergreen coniferous trees at the sites monitored by FFPRI. The mean moisture contents of leaves and branches sampled from the crowns of five konara oak trees in a forest in Kawamata on 26–29 November 2018 were used to model the moisture contents of deciduous broadleaf tree leaves and branches at the sites monitored by FFPRI.

206 **2.2.2 Moisture contents for the organic layer and soil**

207 Moisture contents for the organic layer and soil layers were also based on data from forests
208 in Kawamata and Kawauchi surveyed by JAEA between 2015 and 2017. Samples of the organic
209 layer and soil were taken from Japanese cedar forests in Kawauchi in the periods 1–3 December
210 2015, 18–20 October 2016, 21–23 August 2017 and 16–20 October 2017. Means (n = 10) of
211 the moisture content of the organic layer and 5 cm thick soil layers down to 20 cm depth were
212 used to model the single stand evergreen coniferous species forests monitored by FFPRI (KU1-
213 H, OT-S, TB-H).

214 Data from forests containing deciduous broadleaf species and Japanese red pine trees in
215 Kawamata and Kawauchi surveyed by JAEA was used for modelling the moisture content of
216 the organic layer and soil in the forests monitored by FFPRI with multiple tree species. These
217 surveys took place on 3–8 December 2015, 17–21 October 2016 and 17–31 October 2017.
218 Means (n = 7) of the moisture contents were used in the simulations.

219

220 **2.2.3 Vertical distribution of ^{134}Cs and ^{137}Cs within 5 cm soil layers**

221 The vertical distribution of ^{137}Cs within soil at three forest sites at Yamakiya, Kawamata
222 was monitored by the University of Tsukuba between 2011 and 2017 (Takahashi et al., 2018).
223 The three sites are a mixed forest (MF) of Japanese red pine and konara oak, and a young cedar
224 (YC) and mature cedar (MC) plantation of Japanese cedar. A scraper plate (450 cm^2) area was
225 used to collect soil layers from each site over nine surveys between June 2011 and June 2017.
226 The data all show an approximately exponential decrease in the ^{137}Cs concentration with
227 vertical depth in soil.

228 Following Liu et al. (2019), the cumulative form of the exponential distribution

229 $$I(\zeta) = I_{\mathrm{inv}}(1-\exp(-\zeta/\beta)) \quad (1)$$

was used to fit the cumulative inventory of ^{137}Cs, $I(\zeta)$ (Bq/cm^2), as a function of the cumulative mass depth of wet soil, ζ (g/cm^2). Relaxation mass depth parameters, β (g/cm^2), and total ^{137}Cs inventories, I_{inv} (Bq/cm^2), were extracted from the fits. The fitting was performed using the trust region reflective algorithm for non-linear least squares optimization in the SciPy Python package (Virtanen et al., 2020). Fitted parameters are listed in Table S2 and fits shown in Fig. S1.

Only one set of scraper plate samples was taken at each site per survey and there was a large degree of scatter in the fitted β values between different survey dates (Fig. 1). It is not clear *a priori* that β should increase monotonically over time in forest soils as is the case for open sites (Liu et al., 2019). This is because at open sites the input of ^{134}Cs and ^{137}Cs to the soil surface occurred acutely in March 2011 with the radioactive plumes from the FDNPP accident. For forests, the input of ^{134}Cs and ^{137}Cs into forest soil occurs over a prolonged period, starting with the initial deposition fallout, followed by the transfer of ^{134}Cs and ^{137}Cs from the forest canopy to the organic layer and from the organic layer to soil over many years affected by multiple processes. Given the scatter of the data in Fig. 1 explained by the low number of samples, it was not considered justifiable to fit a linear function for the dependency of β on time to the data.

Instead, the mean values of β from the surveys of the YC and MC sites (n = 18), and from the surveys at the MF site (n = 9), were used to model the distribution of ^{134}Cs and ^{137}Cs within the 5 cm layers at the single stand and multiple stand forests monitored by FFPRI, respectively. It is recognized that this method means the simulations cannot model how temporal changes to the ^{134}Cs and ^{137}Cs mass depth profiles inside the 5 cm forest soil layers affect $\dot{H}^*(10)$. The potential effects of this limitation were therefore assessed with the uncertainty analysis. Note however that the migration of ^{134}Cs and ^{137}Cs between the organic layer and different 5 cm soil

layers is captured by the simulations, as the FFPRI surveys measured the radioactivities of these different layers independently.

2.2.4 Natural background radiation

Results from Andoh et al. (2017) were used to estimate the natural background component in the $\dot{H}^*(10)$ measurements taken with NaI(Tl) scintillator survey meters (TCS-172B) during the FFRPI surveys. Andoh et al. (2017) analyzed gamma spectra measured with KURAMA-II instruments (CsI(Tl) scintillators) (Tanigaki et al., 2015) during car-borne surveys in eastern Japan to separate the natural background component of $\dot{H}^*(10)$ from the ^{134}Cs and ^{137}Cs components. The mean natural background component of $\dot{H}^*(10)$ calculated for Fukushima Prefecture of 0.055 μSv/h (±0.010 μSv/h) was used for modelling the natural background component for the sites in Fukushima Prefecture. The value calculated for Ibaraki Prefecture (0.060±0.006 μSv/h) was used for site TB-H. Note that the natural background component of $\dot{H}^*(10)$ in the measurements taken with the TCS-172B and KURAMA-II survey meters includes contributions from both terrestrial gamma rays and cosmic radiation. The terrestrial component is the dominant component however, as these devices have low sensitivity to cosmic radiation (Nagaoka et al., 1996; Yajima et al., 2014; Andoh et al., 2017).

2.3 Radiation transport simulations

The simulations for $\dot{H}^*(10)$ were undertaken with the Particle and Heavy Ion Transport code System (PHITS) version 3.20, which is a Monte Carlo code (Sato et al., 2018). A model of multiple layers of uniform matter was used to represent forests (Fig. 2). The thickness, density, material composition, and ^{134}Cs and ^{137}Cs radioactivities were set independently for each layer based on the measurements from the various forest samples. The models were created in boxes with reflective boundary conditions for gamma rays at the vertical boundary

faces. This method ensured an effectively infinite area forest was simulated so that the $\dot{H}^*(10)$ estimates would saturate (Malins et al., 2015a; Malins et al., 2015b). It can be used because the model geometry and the ^{134}Cs and ^{137}Cs source distribution has 4-fold rotational symmetry.

The elemental compositions of the materials for each layer were set by combining base components of air, water, organic matter and mineral soil (Table 2). The density of each base component was equal to its respective volumetric density within the layer. Soil was modelled as a mixture of black forest soil (andosol), organic matter and water. The carbon content of dry forest soil (i.e. the black forest soil and organic matter mixture) was set to 10.7% by weight (Kawada, 1982; Kawada, 1989). The organic layer was assumed to contain zero black forest soil. The canopy and trunk layers were modelled as a mixture of dry organic matter, water and air.

The means of the physical data used for each layer in the forest models are summarized in Table 3. The masses per unit area include both the dry material and the moisture masses. For the trunk and canopy layers, the data include the air mass per unit area (calculated using a volumetric density of 1.2 kg/m^3). Note that tree matter only displaces a negligible volume of the atmosphere. Maximum and minimum values of the data are given for the nine sites.

The Electron-Gamma Shower version 5 (EGS5) algorithm in PHITS was used for photon transport (Hirayama et al., 2005; Sato et al., 2018). The data for energies and emission probabilities for gamma rays from ^{134}Cs and ^{137}Cs decay came from the Evaluated Nuclear Structure Data Files (ENSDF). This data was accessed using the Nudat2 (2020) website.

Values of $\dot{H}^*(10)$ were evaluated using track length tallies to calculate photon fluxes, then these were converted to $\dot{H}^*(10)$ using conversion coefficients from ICRP (1996). Tally regions were thin layers set at 0.1, 1 and 20 m above the ground (dashed lines, Fig. 2). Monte Carlo statistical uncertainties for calculated $\dot{H}^*(10)$ were lower than 0.1%.

The minimum energy cut off for photon transport in EGS5 was set at 3 keV. For computational efficiency secondary particles from photon interactions (electrons, positrons and Bremsstrahlung) were not generated and transported in the simulations. The effect of this simplification was checked by repeating one simulation will full transport of all particles (photons, electrons, positrons and Bremsstrahlung) down to 1 keV. The difference in the simulated $\dot{H}^*(10)$ between the two cases was negligible.

2.4 Analysis of uncertainties

The uncertainties in the parameters derived from the field measurements that were used as simulation inputs were characterized as follows. Standard errors of measurements were used to represent the uncertainties when the measurements were taken at the same site and in the same year as the case being simulated. Standard deviations were used otherwise, i.e. for the scenarios where specific measurements for that site and year were not available, so the data had to be estimated using measurements taken in other years or from other sites. This is because the plausible distributions of the unmeasured values are better represented by standard deviations of the proxy measurements than standard errors.

The uncertainties in the simulation results for $\dot{H}^*(10)$ that propagate from the uncertainties in the measured input variables were assessed as follows. It was assumed that the distributions of the measurement uncertainties were Gaussian. For each site and year, multiple simulations were performed with the input variables drawn randomly from the uncertainty distributions. For simplicity it was assumed that the uncertainties for each variable were uncorrelated. The exception to this was the ^{134}Cs and ^{137}Cs radioactivity measurements of each component, which were assumed to be perfectly correlated to keep the ^{134}Cs/^{137}Cs ratio fixed.

Total uncertainties in the simulated $\dot{H}^*(10)$ were calculated using the above method by varying all input variables randomly within their respective uncertainty distributions. To

understand the contributions from different input uncertainties to the total uncertainty, further simulations were performed for sites OT-Q, OT-S and TB-H for 2011 and 2016 varying only a single class of input variables randomly within their uncertainty distributions. It was found that performing 100 simulations with randomly drawn input variables was sufficient to converge the uncertainty estimates for the simulated $\dot{H}^*(10)$ (Fig. 3).

3. Results and discussion

3.1 Comparison of simulated and measured ambient dose equivalent rates

There was a clear correspondence between the simulated $\dot{H}^*(10)$ and the measurements taken with handheld NaI(Tl) scintillator survey meters (Fig. 4). All simulation results were within a factor of two of the measurements. The mean absolute percentage deviations of the simulations from the measurements were respectively 24% and 22% for $\dot{H}^*(10)$ at 0.1 and 1 m above the ground (Table 4).

The correlation between simulated and measured $\dot{H}^*(10)$ in this study compares favorably against a previous study simulating $\dot{H}^*(10)$ at open sites, such as farmland, grass fields and parks (Malins et al., 2016). In that study the mean absolute percentage deviation of the simulations from measurements was 29%, and the coefficient of determination (R^2) was 0.825. The range of dose rates at sites in both studies was similar (0.05 to 5 μSv/h). As the modelling methods and complexity were broadly comparable between the two studies, the better correlation obtained in this study is attributable to the lower uncertainties in inputs to the simulations. The simulations in Malins et al. (2016) were based on a single scraper plate sample set taken at each site. In comparison in this study the simulation inputs were typically averages of n = 3 to 6 replicated measurements taken at each site per survey.

There was also better agreement between simulated and measured $\dot{H}^*(10)$ in this study than a recent study which created 3D Monte Carlo models of sites in Fukushima Prefecture

353 with individual buildings and trees tailored to specific sites (Kim et al., 2019). Again the likely
354 explanation for this is the lower measurement uncertainties in the inputs to the models in this
355 study due to more replications of measurements.
356
357 **3.2 Breakdown of different source contributions to ambient dose equivalent rates**
358 Breakdowns of the contributions to the simulated $\dot{H}^*(10)$ at 1 m above the ground from
359 ^{134}Cs and ^{137}Cs located in different parts of the forests and from natural background radiation
360 are shown in Fig. 5. The largest contributors to simulated $\dot{H}^*(10)$ over the study periods were
361 ^{134}Cs and ^{137}Cs located in the canopy, organic layer and top 5 cm of soil, as well as natural
362 background radiation for sites with low overall ^{134}Cs and ^{137}Cs radioactivity levels like TB-H
363 and TD-S.
364 Contributions from ^{134}Cs and ^{137}Cs in the canopy were greatest in 2011 and 2012, as the
365 interception of atmospheric fallout by the canopy in March 2011 meant the radioactivity of the
366 canopy was highest in the first two years (Fig. 6). The radioactivity in the canopy transferred
367 to the forest floor due to throughfall, litterfall and stemflow in the years following the fallout in
368 2011 (Teramage et al., 2014; Endo et al., 2015; Kato et al., 2017; Imamura et al., 2017b). This
369 meant the contributions from radioactivity in the canopy to $\dot{H}^*(10)$ decreased substantially in
370 later years of the study periods (Fig. 5).
371 There were large contributions to simulated $\dot{H}^*(10)$ from ^{134}Cs and ^{137}Cs in the organic
372 layer and top 5 cm of soil from 2011 onwards (Fig. 5). The transfer of ^{134}Cs and ^{137}Cs in the
373 organic layer to the top 5 cm of soil occurs more gradually than from the canopy to the forest
374 floor (Hashimoto et al., 2020), cf. Fig. 6. This meant that, setting aside the contribution from
375 natural background radiation at the lower dose rate sites, there was a slow change to radioactive
376 cesium within the top 5 cm of soil becoming the main contributor to $\dot{H}^*(10)$ by 2016 and 2017
377 (Fig. 5).

The relative contribution of ^{134}Cs and ^{137}Cs in the organic layer to simulated $\dot{H}^*(10)$ becoming progressively smaller over time underlies why decontaminating forests by removing the organic layer becomes less effective the later it is conducted (Koarashi et al., 2020). Unless the organic layer is replaced by a fresh layer of uncontaminated material, e.g. wood chips (Cresswell et al., 2016), removing it in the later years of the 2011–17 study period will undercover more highly radioactive soil beneath the organic layer. The loss of shielding of this soil by the organic layer will then act counteractively to the benefit of removing the ^{134}Cs and ^{137}Cs inventory associated with the organic layer from the forest.

Cesium-134 and ^{137}Cs located in tree trunks and in soil between 5 and 20 cm depths makes a minor contribution to $\dot{H}^*(10)$ for all sites and years simulated (Fig. 5). The former is explained by the low quantity of ^{134}Cs and ^{137}Cs contained within trunks for all years (Fig. 6), which is typically less than 3% of the total radioactivity of ^{134}Cs and ^{137}Cs in the forests (Imamura et al., 2017b). For the latter, the quantity of ^{134}Cs and ^{137}Cs within soil between 5 and 20 cm depths only attains around 15% of the total forest ^{134}Cs and ^{137}Cs inventory by 2016 and 2017 (Fig. 6). The self-shielding of these gamma rays by the topsoil means ^{134}Cs and ^{137}Cs in soil between 5 and 20 cm depths only contributes to 8–10% of the total $\dot{H}^*(10)$ in 2016 and 2017.

The relative contribution form natural background radiation ranges from 3.8% (KU1-S, 2011) to 63% (TD-S, 2015) of the total $\dot{H}^*(10)$ for the sites surveyed. In all cases the relative importance of the background contribution increases over time as radioactive decay reduces the quantities of ^{134}Cs and ^{137}Cs in the forests.

Fig. 7 shows the contributions to simulated $\dot{H}^*(10)$ at 20 m above the ground. This height was chosen for analysis as it is above the upper canopy of all the forests and is a typical height for the operation of unmanned vehicles in aerial radiation surveys (Ochi et al., 2019). The relative importance of ^{134}Cs and ^{137}Cs within the canopy to $\dot{H}^*(10)$ above it is larger than for

$\dot{H}^*(10)$ near ground level (cf. Figs. 5 and 7). The canopy contribution is on average 48% of the total contribution from ^{134}Cs and ^{137}Cs to $\dot{H}^*(10)$ at 20 m in 2011, decreasing to 8.9% by 2014. The simulated $\dot{H}^*(10)$ above the canopy decreased at a faster rate than at ground level following fallout, consistent with modelling by Gonze et al. (2016). This effect may need to be accounted for in the analysis of airborne survey results performed in different years following radioactive fallout events (Kato et al., 2019).

3.3 Effects of uncertainties in input measurements on simulations

The mean relative uncertainty in simulated $\dot{H}^*(10)$ at 1 m above the ground due to the measurement uncertainties in the model inputs was 11%. This was four times greater than the mean relative uncertainty, 2.8%, in the $\dot{H}^*(10)$ measurements at 1 m. The breakdown of factors contributing to the overall simulation uncertainty is shown for three sites for 2011 and 2016 in Fig. 8 (right vertical axis).

The main contributors to the overall simulation uncertainties were the measurement uncertainties in the ^{134}Cs and ^{137}Cs radioactivity of the top 5 cm of soil, the organic layer and the canopy, the relaxation mass depth parameter β for the distribution of ^{134}Cs and ^{137}Cs in the 5 cm soil layers, and the natural background contribution to $\dot{H}^*(10)$. This reflects both the high relative uncertainties in the measurements underlying these inputs (shown by black dots and lines, left vertical axis in Fig. 8), and that the majority of the ^{134}Cs and ^{137}Cs in the forests was contained in these layers over the study period.

The uncertainty in the distribution of ^{134}Cs and ^{137}Cs with mass depth in the 5 cm soil layers has an increasingly important effect as ^{134}Cs and ^{137}Cs enters the topsoil in the years following the fallout. In this study the relaxation mass depth parameter (β) was fixed for each site for all simulated years. By consequence of linking the vertical distribution of ^{134}Cs and ^{137}Cs within each 5 cm soil layer to β, the input uncertainties in the dry density and moisture

content of the soil layers had negligible effect on the simulated $\dot{H}^*(10)$ results. This is because the ^{134}Cs and ^{137}Cs mass depth distribution that is most important factor determining the gamma ray fluence in the air (ICRU, 1994) and keeping β fixed means the ^{134}Cs and ^{137}Cs mass depth distribution in soil remains unchanged if the soil dry density or moisture content are varied.

In reality the vertical distribution of ^{134}Cs and ^{137}Cs within forest soil varies on the centimeter scale over time (Muto et al., 2019) and this potentially affects ambient dose equivalent rates in forests in a similar manner to open sites (Mikami et al., 2015b). Understanding the importance of this effect on $\dot{H}^*(10)$ in forests remains an open question that will require better data on the temporal dependency of the vertical distribution of ^{134}Cs and ^{137}Cs in forests soil over time to resolve. However, the results of Fig. 8 suggest that variations in the relaxation mass depth parameter β between approximately 0.5 to 2 g/cm^2 in forest soils affects $\dot{H}^*(10)$ on the order of 5%. On a timescale of decades, the radioactive cesium distribution in forest soil may tend towards a more uniform distribution due to root decomposition (Sakashita et al., 2020). Monitoring studies of the radioactive cesium distribution in forest soil will therefore be important over the long term.

The uncertainty in the natural background contribution to $\dot{H}^*(10)$ at these sites (Fig. 8) could be reduced by performing in situ gamma spectroscopy measurements at the sites and calculating the natural background contribution from the measured spectrum (Clouvas et al., 1999; Cresswell et al., 2016). This would reduce the uncertainties that arose from using the data from car-borne surveys aggregated at district and prefectural levels (Andoh et al., 2017) to infer this component for these models.

4. Conclusions

Monte Carlo radiation transport simulations were performed for ambient dose equivalent rates in nine forests in eastern Japan for 2011 to 2017. The simulation inputs were set using

453 measurements from forests in eastern Japan. The measurement data used included dry densities,
454 moisture contents and ^{134}Cs and ^{137}Cs inventories of different forest compartments.

455 There was a good correspondence between simulated $\dot{H}^*(10)$ and NaI(Tl) scintillator
456 survey meter measurements. The correlation between simulated and measured $\dot{H}^*(10)$ was
457 better in this study on forests than in previous studies modelling $\dot{H}^*(10)$ at open sites and
458 suburban locations (Malins et al., 2016; Kim et al., 2019). This was attributed to more
459 replications of measurements underlying the input data in the models in this study.

460 The calculation results in this study suggest that in 2011 ^{134}Cs and ^{137}Cs in the canopy,
461 organic layer and top 5 cm of soil were the main contributors to the elevated ambient dose
462 equivalent rates at 1 m above the ground in these forests in eastern Japan. By 2014 the organic
463 layer and top 5 cm of soil were the main contributors to $\dot{H}^*(10)$ at 1 m above the ground
464 (excluding natural background) as by then most ^{134}Cs and ^{137}Cs fallout intercepted by the
465 canopy had migrated to the forest floor. By 2016 and 2017 ^{134}Cs and ^{137}Cs in the top 5 cm of
466 forest soil had become the dominant contributor to $\dot{H}^*(10)$ at 1 m.

467 Uncertainties in the simulation results were derived assuming the measurement
468 uncertainties in the model inputs had Gaussian distributions. The measurement uncertainties in
469 the ^{134}Cs and ^{137}Cs radioactivity of the top 5 cm of soil, the organic layer and canopy, the
470 distribution of ^{134}Cs and ^{137}Cs within 5 cm soil layers and the natural background component
471 were the main contributors to the total uncertainties in simulated $\dot{H}^*(10)$. Better
472 characterization of the distribution of ^{134}Cs and ^{137}Cs with mass depth in soil, and site-specific
473 evaluation of natural background contributions to $\dot{H}^*(10)$ using in-situ gamma spectroscopy,
474 would help lower the modelling uncertainties. The former is especially important post-2017
475 due to ^{134}Cs and ^{137}Cs in the top 5 cm of soil being the main contributor to $\dot{H}^*(10)$ at 1 m above
476 the ground.

477

478 **Acknowledgements**

479 The authors thank researchers in the Department of Plant Ecology, the Department of
480 Forest Vegetation, the Department of Forest Soils and the Department of Wood Properties and
481 Processing of FFPRI for allowing their datasets to be used for this research. We thank Dr.
482 Kimiaki Saito for advice and comments on the manuscript. We also thank colleagues in the
483 Center for Computational Science & e-Systems and the Environmental Research Group of
484 CLADS within JAEA for their support. The simulations were performed on JAEA's SGI ICEX
485 supercomputer.

486

487 **References**

488 AIST (National Institute of Advanced Industrial Science and Technology), 2018. GSJ certified
489 geochemical reference material JSO-1 Soil (Black forest soil). (In Japanese)
490 https://gbank.gsj.jp/geostandards/ Accessed date: 4 June 2020.

491 Andoh, M., Matsuda, N., Saito, K., 2017. Evaluation of Ambient Dose Equivalent Rates Owing
492 to Natural Radioactive Nuclides in Eastern Japan by Car-Borne Surveys Using
493 KURAMA–II. Trans. At. Energy Soc. Jpn. 16, 63-80. DOI:10.3327/taesj.J16.023

494 Beck, H.L., DeCampo, J., Gogolak, C., 1972. In Situ Ge(Li) and NaI(Tl) Gamma-Ray
495 Spectrometry. U. S. Atomic Energy Commission. Technical Report HASL-258.
496 DOI:10.2172/4599415

497 Bellamy, M.B., Dewji, S.A., Leggett, R.W., Hiller, M., Veinot, K., Manger, R.P., Eckerman,
498 K.F., Ryman, J.C., Easterly, C.E., Hertel, N.E., Stewart, D.J., 2018. Federal Guidance
499 Report No. 15: External Exposure External Dose Rate Coefficients for General
500 Application. United States Environmental Protection Agency EPA 402-R-18-001.

501 Clouvas, A., Xanthos, S., Antonopoulos-Domis, M., Alifragis, D.A., 1999. Contribution of the
502 ^{137}Cs to the Total Absorbed Gamma Dose Rate in Air in a Greek Forest Ecosystem:
503 Measurements and Monte Carlo Computations. Health Phys. 76, 36-43.
504 Clouvas, A., Xanthos, S., Antonopoulos-Domis, M., Alifragis, D.A., 2005. Radiocesium
505 gamma dose rates in a Greek pine forest: measurements and Monte Carlo computations.
506 Radioact. Environ. 7, 1155-1166. DOI:10.1016/S1569-4860(04)07142-6
507 Cresswell A., Kato, H., Onda, Y., Nanba, K., 2016. Evaluation of forest decontamination using
508 radiometric measurements. J. Environ. Radioact. 164, 133-144.
509 DOI:10.1016/j.jenvrad.2016.07.024
510 Cresswell, A.C., Sanderson, D.C.W., Yamaguchi, K., 2018. Assessment of the calibration of
511 gamma spectrometry systems in forest environments. J. Environ. Radioact. 181, 70-77.
512 DOI:10.1016/j.jenvrad.2017.10.019
513 Endo, I., Ohte, N., Iseda, K., Tanoi, K., Hirose, A., Kobayashi, N.I., Murakami, M., Tokuchi,
514 N., Ohashi, M., 2015. Estimation of radioactive 137-cesium transportation by litterfall,
515 stemflow and throughfall in the forests of Fukushima. J. Environ. Radioact. 149, 176-185.
516 DOI: 10.1016/j.jenvrad.2015.07.027
517 Evrard, O., Laceby, J.P., Lepage, H., Onda, Y., Cerdan, O., Ayrault, S., 2015. Radiocesium
518 transfer from hillslopes to the Pacific Ocean after the Fukushima Nuclear Power Plant
519 accident: A review. J. Environ. Radioact. 148, 92-110.
520 DOI:10.1016/j.jenvrad.2015.06.018
521 Forestry Agency of Japan, 2012. Summary Table of Forest Resources as of 31 March 2012,
522 Forestry Agency, Ministry of Agriculture, Forestry and Fisheries. (In Japanese).
523 https://www.rinya.maff.go.jp/j/keikaku/genkyou/h24/index.html Accessed date: 13 April
524 2020.

525 Forestry Agency of Japan, 2017. Concerning the results of the 2016 survey on the distribution
526 of radioactive materials in forests Forestry Agency, Ministry of Agriculture, Forestry and
527 Fisheries. (In Japanese)
528 https://www.rinya.maff.go.jp/j/kaihatu/jyosen/H28_jittaihaaku_kekka.html Accessed
529 date: 4 June 2020.
530 Forestry Agency of Japan, 2018. Concerning the results of the 2017 survey on the distribution
531 of radioactive materials in forests Forestry Agency, Ministry of Agriculture, Forestry and
532 Fisheries. (In Japanese)
533 https://www.rinya.maff.go.jp/j/kaihatu/jyosen/H29_jittaihaaku.html Accessed date: 4
534 June 2020.
535 Fujii, K., Ikeda, S., Akama, A., Komatsu, M., Takahashi, M., Kaneko, S., 2014. Vertical
536 migration of radiocesium and clay mineral composition in five forest soils contaminated
537 by the Fukushima nuclear accident. Soil Sci. Plant Nutr. 60, 751-764.
538 DOI:10.1080/00380768.2014.926781
539 Fukushima, K., 2010, Chemical Composition of Wood. Japan Wood Research Society,
540 Chemistry of Wood. Bun-eido Shuppan, Tokyo, 1-4, p339. (In Japanese)
541 Gering, F., Kiefer, P., Fesenko, S., Voigt, G., 2002. In situ gamma-ray spectrometry in forests:
542 Determination of kerma rate in air from ^{137}Cs. J. Environ. Radioact. 61, 75-89.
543 DOI:10.1016/S0265-931X(01)00116-3
544 Golikov, V., Barkovski, A., Kulikov, V., Balonov, M., Rantavaara, A., Vetikko, V., 1999.
545 Gamma Ray Exposure Due to Sources in the Contaminated Forest. In Contaminated
546 Forests. NATO Science Series (Series 2: Environmental Security), 58, 333-341, Springer,
547 Dordrecht. DOI:10.1007/978-94-011-4694-4_35

548 Gonze, M.A., Mourlon, C., Calmon, P., Manach, E., Debayle, C., Baccou, J., 2016. Modelling
549 the dynamics of ambient dose rates induced by radiocaesium in the Fukushima terrestrial
550 environment. J. Environ. Radioact. 161, 22-34. DOI:10.1016/j.jenvrad.2015.06.003
551 Haraguchi, T., Terashima, N., Usuda, M., Koshijima, T., Sakai, K., Morohoshi, N., Kai, Y.,
552 Shimizu, K., Sakakihara, A., 1985. Chemistry of Wood. Bun-eido Shuppan, Tokyo, p288.
553 (In Japanese)
554 Hashimoto, S., Ugawa, S., Nanko, K., Shichi, K., 2012. The total amounts of radioactively
555 contaminated materials in forests in Fukushima, Japan. Sci. Rep. 2, 416.
556 DOI:10.1038/srep00416
557 Hashimoto, S., Imamura, N., Kaneko, S., Komatsu, M., Matsuura, T., Nishina, K., Ohashi, S.,
558 2020. New predictions of ^{137}Cs dynamics in forests after the Fukushima nuclear accident.
559 Sci. Rep. 10, 29. DOI:10.1038/s41598-019-56800-5
560 Hemmi, K., Yamaguchi, T., Takeda, S., Kimura, H., 2017. Analysis on the effect of forest
561 decontamination on reducing the air dose rate using the three-dimensional transport code
562 MCNP. J. Nucl. Fuel Cycle Environ. 24, 3-14 (In Japanese with English abstract).
563 DOI:10.3327/jnuce.24.1_3
564 Hirayama, H., Namito, Y., Bielajew, A.F., Wilderman, S.J., Nelson, W.R., 2005. The EGS5
565 Code System. SLAC-R-730 and KEK Report 2005-8.
566 ICRP, 1996. ICRP Publication 74: Conversion coefficients for use in radiological Protection
567 against external radiation. Ann. ICRP 26, 1-205. DOI:10.1016/S0146-6453(96)90010-X
568 ICRU, 1994. Gamma-ray spectrometry in the environment. ICRU Report 53.
569 Ikeda, S., Kaneko, S., Akama, A., Takahashi, M., 2014. Methods for assessing the spatial
570 distribution and dynamics of radiocesium in forest soils. Bull. For. For. Prod. Res. Inst. 13,
571 137-145. (In Japanese with English abstract)

572 Imamura, N., Kaneko, S., Kobayashi, M., Takahashi, M., Akama, A., 2015. Change of air dose
573 rate in forests from 2011 to 2014 after the Fukushima Daiichi nuclear power plant accident.
574 Jpn. J. For. Environ. 57, 101-107. (In Japanese with English abstract)
575 DOI:10.18922/jjfe.57.2_101
576 Imamura, N., Akama, A., Ohtani, Y., Kobayashi, M., Tsuboyama, Y., Takahasi, M., 2017a. An
577 estimation of air dose rate from considering of radiocesium distribution in Japanese forests.
578 J. Jpn. For. Soc. 99, 1-9. (In Japanese with English abstract) DOI:10.4005/jjfs.99.1
579 Imamura, N., Komatsu, M., Ohashi, S., Hashimoto, S., Kajimoto, T., Kaneko S., Takano, T.,
580 2017b. Temporal changes in the radiocesium distribution in forests over the five years
581 after the Fukushima Daiichi Nuclear Power Plant accident. Sci. Rep. 7, 8179.
582 DOI:10.1038/s41598-017-08261-x
583 Kajimoto, T., Takano, T., Saito, S., Kuroda, K., Fujiwara, T., Komatsu, M., Kawasaki, T.,
584 Ohashi, S., Kiyono, Y., 2014. Methods for assessing the spatial distribution and dynamics
585 of radiocesium in tree components in forest ecosystems. Bull. For. For. Prod. Res. Inst. 13,
586 113-136. (In Japanese with English abstract)
587 Karadeniz, O., Çakir, R. Karakurt, H., 2015. Estimation of vertical migration velocity of ^{137}Cs
588 in the Mount IDA/Kazdagi, Turkey. J. Environ. Radioact. 146, 27-34.
589 DOI:10.1016/j.jenvrad.2015.03.032
590 Kato, H., Onda, Y., Hisaome, K., Loffredo, N., Kawamori, A., 2017. Temporal changes in
591 radiocesium deposition in various forest stands following the Fukushima Dai-ichi
592 Nuclear Power Plant accident. J. Envrion. Radioact. 166, 449-457.
593 DOI:10.1016/j.jenvrad.2015.04.016
594 Kato, H., Onda, Y., Gao, X., Sanada, Y., Saito, K., 2019. Reconstruction of a Fukushima
595 accident-derived radiocesium fallout map for environmental transfer studies. J. Environ.
596 Radioact. 210, 105996. DOI:10.1016/j.jenvrad.2019.105996

597 Kawada, H., 1982. Chemical Characteristics of Soils. Forest Soil Research Group,
598 Investigation Methods of Forest Soils and their Properties. Rinya Kousaikai, Tokyo, 238-
599 272. (In Japanese)
600 Kawada, H., 1989. Introduction to Forest Soil Science. Hakuyusha, Tokyo, p399. (In
601 Japanese)
602 Kenzo, T., Saito, S., Araki, M.G., Kajimoto, T., K., 2020. Vertical distribution of radiocesium
603 concentrations among crown positions and year-to-year variation in four major tree
604 species after the Fukushima Daiichi Nuclear Power Plant accident. J. Environ. Radioact.
605 225, 106447. DOI:10.1016/j.jenvrad.2020.106447
606 Kim, M., Malins, A., Yoshimura, K., Sakuma, K., Kurikami, H., Kitamura, A., Machida, M.,
607 Hasegawa, Y., Yanagi, H., 2019. Simulation study of the effects of buildings, trees and
608 paved surfaces on ambient dose equivalent rates outdoors at three suburban sites near
609 Fukushima Dai-ichi. J. Environ. Radioact. DOI:10.1016/j.jenvrad.2018.09.001
610 Koarashi, J., Atarashi-Andoh, M., Nishimura, S., Muto, K., 2020. Effectiveness of
611 decontamination by litter removal in Japanese forest ecosystems affected by the
612 Fukushima nuclear accident. Sci. Rep. 10, 6614. DOI:10.1038/s41598-020-63520-8
613 Komatsu, M., Kaneko, S., Ohashi, S., Kuroda, K., Sano, T., Ikeda, S., Saito, S., Kiyono, Y.,
614 Tonosaki, M., Miura, S., Akama, A., Kajimoto, T., Takahashi, M., 2016. Characteristics
615 of initial deposition and behavior of radiocesium in forest ecosystems of different locations
616 and species affected by the Fukushima Daiichi Nuclear Power Plant accident. J. Environ.
617 Radioact. 161, 2-10. DOI:10.1016/j.jenvrad.2015.09.016
618 Kurikami, H., Sakuma, K., Malins, A., Sasaki, Y., Niizato, T., 2019. Numerical study of
619 transport pathways of ^{137}Cs from forests to freshwater fish living in mountain streams in
620 Fukushima, Japan. J. Environ. Radioact. 208-209, 106005.
621 DOI:10.1016/j.jenvrad.2019.106005

622 Kuroda, K., Kagawa, A., Tonosaki, M., 2013. Radiocesium concentrations in the bark, sapwood
623 and heartwood of three tree species collected at Fukushima forests half a year after the
624 Fukushima Dai-ichi nuclear accident. J. Environ. Radioact. 122, 37-42.
625 DOI:10.1016/j.jenvrad.2013.02.019
626 Liu, X., Machida, M., Kurikami, H., Kitamura, A., 2019. Long-term simulations of radiocesium
627 discharge in watershed with improved radioesium wash-off model: Applying the model to
628 Abukuma River basin of Fukushima. J. Environ. Radioact. 203, 135-146.
629 DOI:10.1016/j.jenvrad.2019.03.001
630 Malins, A., Machida, M., Saito, K., 2015a. Comment on 'Update of ^{40}K and ^{226}Ra and ^{232}Th
631 series γ-to-dose conversion factors for soil'. J. Environ. Radioact. 144, 179-180.
632 DOI:10.1016/j.jenvrad.2015.01.009
633 Malins, A., Okumura, M., Machida, M., Takemiya, H., Saito, K., 2015b. Fields of View for
634 Environmental Radioactivity. In Proceedings of the International Symposium on
635 Radiological Issues for Fukushima's Revitalized Future. arXiv:1509.09125v2
636 Malins, A., Kurikami, H., Nakama, S., Saito, T., Okumura, M., Machida, M., 2016. Evaluation
637 of ambient dose equivalent rates influenced by vertical and horizontal distribution of
638 radioactive cesium in soil in Fukushima Prefecture. J. Environ. Radioact. 151, 38-49.
639 DOI:10.1016/j.jenvrad.2015.09.014
640 Manaka, T., Imamura, N., Kaneko, S., Miura, S., Furusawa, H., Kanasashi, T., 2019. Six-year
641 trends in exchangeable radiocesium in Fukushima forest soils. J. Environ. Radioact. 203,
642 84-92. DOI:10.1016/j.jenvrad.2019.02.014
643 Mikami, S., Maeyama, T., Hoshide, Y., Sakamoto, R., Sato, S., Okuda, N., Demongeot, S.,
644 Gurriaran, R., Uwamino, Y., Kato, H., Fujiwara, M., Sato, T., Takemiya, H., Saito, K.,
645 2015a. Spatial distributions of radionuclides deposited onto ground soil around the

Fukushima Dai-ichi Nuclear Power Plant and their temporal change until December 2012. J. Environ. Radioact. 139, 320-343. DOI:10.1016/j.jenvrad.2014.09.010

Mikami, S., Maeyama, T., Hoshide, Y., Sakamoto, R., Sato, S., Okuda, N., Sato, T., Takemiya, H., Saito, K., 2015b. The air dose rate around the Fukushima Dai-ichi nuclear power Plant: its spatial characteristics and temporal changes until December 2012. J. Environ. Radioact. 139, 250-259. DOI:10.1016/ j.jenvrad.2014.08.020.

Miller, K.M., Kuiper, J.L., Helfer, I.K., 1990. ^{137}Cs fallout depth distributions in forest versus field sites: Implications for external gamma dose rates. J. Environ. Radioact. 12, 23-47. DOI:10.1016/0265-931X(90)90034-S

Mishra, S., Sahoo, S.K., Bossew, P., Sorimachi, A., Tokonami, S., 2016. Vertical migration of radio-caesium derived from the Fukushima Dai-ichi Nuclear Power Plant accident in undisturbed soils of grassland and forest. J. Geochem. Explor. 169, 163-186. DOI:10.1016/j.gexplo.2016.07.023

Miura, S., 2016. The Effects of Radioactive Contamination on the Forestry Industry and Commercial Mushroom-Log Production in Fukushima, Japan. In: Nakanishi, T.M., Tanoi, K. (Eds.), Agricultural Implications of the Fukushima Nuclear Accident the First Three Years. Springer, pp. 145-160. DOI:10.1007/978-4-431-55828-6_12

Muto, K., Atarashi-Andoh, M., Matsunaga, T., Koarashi, J., 2019. Characterizing vertical migration of ^{137}Cs in organic layer and mineral soil in Japanese forests: Four-year observation and model analysis. J. Environ. Radioact. 208-209, 106040. DOI:10.1016/j.jenvrad.2019.106040

Nagaoka, K., Honda, K., Miyano, K., 1996. Cosmic-ray Contribution in Measurement of Environmental Gamma-ray Dose. Radioisot. 45, 665-674. DOI:10.3769/radioisotopes.45.11_665

Niizato, T., Abe, H., Mitachi, K., Sasaki, Y., Ishii, Y., Watanabe, T., 2016. Input and output budgets of radiocesium concerning the forest floor in the mountain forest of Fukushima released from the TEPCO's Fukushima Dai-ichi nuclear power plant accident. J. Environ. Radioact. 161, 11-21. DOI:10.1016/j.jenvrad.2016.04.017

NuDat2, 2020. Software to search and plot nuclear structure and decay data interactively. Version 2.8. Employs data from the Evaluated Nuclear Structure Data File (ENSDF). http://www.nndc.bnl.gov/nudat2/, Accessed date: 22 May 2020.

Ochi, K., Sasaki, M., Ishida, M., Sanada, Y., 2019. Comparison of airborne and ground-based tools used for radiation measurement in the environment. Prog. Nucl. Sci. Technol. 6, 103-107.

Ohashi, S., Kuroda, K., Takano, T., Suzuki, Y., Fujiwara, T., Abe, H., Kagawa, A., Sugiyama, M., Kubojima, Y., Zhang, C., Yamamoto, K., 2017. Temporal trends in ^{137}Cs concentrations in the bark, sapwood, heartwood, and whole wood of four tree species in Japanese forests from 2011 to 2016. J. Environ. Radioact. 178-179, 335-342. DOI:10.1016/j.jenvrad.2017.09.008

Saito, K., Jacob, P., 1995. Gamma Ray Fields in the Air Due to Sources in the Ground. Rad. Prot. Dosim. 58, 29-45. DOI:10.1093/oxfordjournals.rpd.a082594

Saito, K., Petoussi-Henss, N., 2014. Ambient dose equivalent conversion coefficients for radionuclides exponentially distributed in the ground. J. Nucl. Sci. Technol. 51, 1274-1287. DOI:10.1080/00223131

Sakashita, W., Miura, S., Akama, A., Ohashi, S., Ikeda, S., Saitoh, T., Komatsu, M., Shinomiya, Y., Kaneko, S., 2020. Assessment of vertical radiocesium transfer in soil via roots. J. Environ. Radioact. 222, 106369. DOI:10.1016/j.jenvrad.2020.106369

Sakuma, K., Tsuji, H., Hayashi, S., Funaki, H., Malins, A., Yoshimura, K., Kurikami, H., Kitamura, A., Iijima, K., Hosomi, M., 2018a. Applicability of K_d for modelling dissolved

695 ^{137}Cs concentrations in Fukushima river water: Case study of the upstream Ota River. J.
696 Environ. Radioact. 184-185, 53-62. DOI:10.1016/j.jenvrad.2018.01.001
697 Sakuma, K., Niizato, T., Kim, M., Malins, A., Machida, M., Yoshimura, K., Kurikami, H.,
698 Kitamura, A., Hosomi, M., 2018b. Development of an Evaluation Tool for Air Dose Rate
699 in Forests Using a Monte Carlo Radiation Transport Code (PHITS). Jpn. J. Soc.
700 Remediation Radioact. Contam. Environ. 6, 145-152 (In Japanese with English abstract).
701 Sanada, Y., Sugita, T., Nishizawa, Y., Kondo, A., Torii, T., 2014. The aerial radiation
702 monitoring in Japan after the Fukushima Daiichi nuclear power plant accident. Prog. Nucl.
703 Sci. Technol. 4, 76-80. DOI:10.15669/pnst.4.76
704 Sato, T., Iwamoto, Y., Hashimoto, S., Ogawa, T., Furuta, T., Abe, S., Kai, T., Tsai, P., Matsuda,
705 N., Iwase, H., Shigyo, N., Sihver, L., Niita, K., 2018. Features of Particle and Heavy Ion
706 Transport code System (PHITS) version 3.02. J. Nucl. Sci. Technol. *online ahead of print*.
707 DOI:10.1080/00223131.2017.1419890
708 Takahashi, J., Onda, Y., Hihara, D., Tamura, K., 2018. Six-year monitoring of the vertical
709 distribution of radiocesium in three forest soils after the Fukushima Dai-ichi Nuclear
710 Power Plant accident. J. Environ. Radioact. 192, 172-180.
711 DOI:10.1016/j.jenvrad.2018.06.015
712 Tanigaki, M., Okumura, R., Takamiya, K., Sato, N., Yoshino, H., Yoshinaga, H., Kobayashi,
713 Y., Uehara, A., Yamana, H., 2015. Development of KURAMA-II and its operation in
714 Fukushima. Nucl. Instrum. Methods Phys. Rev. A 781, 57-64.
715 DOI:10.1016/j.nima.2015.01.086
716 Teramage, M.T., Onda, Y., Kato, H., Gomi, T., 2014. The role of litterfall in transferring
717 Fukushima-derived radiocesium to a coniferous forest floor. Sci. Total Environ. 490, 430-
718 439. DOI:10.1016/j.scitotenv.2014.05.034

719 Teramage, M.T., Onda, Y., Kato, H., 2016. Small scale temporal distribution of radiocesium in
720 undisturbed coniferous forest soil: Radiocesium depth distribution profiles. J. Envrion.
721 Manag. 170, 97-104. DOI:10.1016/j.jenvman.2016.01.014
722 Teramage, M.T., Sun, X., 2020. Dosimetric depth distribution of Fukushima-derived ^{137}Cs in
723 coniferous forest soil. J. Radioanal. Nuc. Chem. 323, 233-239. DOI:10.1007/s10967-019-
724 06868-0
725 UNSCEAR, 2000. Sources, Effects and Risks of Ionizing Radiation, UNSCEAR 2000 Report,
726 Volume I: Sources.
727 Wada, T., Konoplev, A., Wakiyama, Y., Watanabe, K., Furuta, Y., Morishita, D., Kawata, G.,
728 Nanba, K., 2019. Strong contrast of cesium radioactivity between marine and freshwater
729 fish in Fukushima. J. Environ. Radioact. 204, 132-142.
730 DOI:10.1016/j.jenvrad.2019.04.006
731 Virtanen, P., Gommers, R., Oliphant, T.E., Haberland, M., Reddy, T., Cournapeau, D.,
732 Burovski, E., Peterson, P., Weckesser, W., Bright, J., van der Walt, S.J., Brett, M., Wilson,
733 J., Millman, K.J., Mayorov, N., Nelson, A.R.J., Jones, E., Kern, R., Larson, E., Carey, C.J.,
734 Polat, I., Feng, Y., Moore, E.W., VanderPlas, J., Laxalde, D., Perktold, J., Cimrman, R.,
735 Henriksen, I., Quintero, E.A., Harris, C.R., Archibald, A.M., Ribeiro, A.H., Pedregosa, F.,
736 van Mulbregt, P. et al., 2020. SciPy 1.0: fundamental algorithms for scientific computing
737 in Python. Nat. Meth. 17, 261-272. DOI:10.1038/s41592-019-0686-2
738 Yajima, K., Iwaoka, K., Yasuda, H., 2014. Radiation Survey Along Two Trails in Mt. Fuji to
739 Investigate the Radioactive Contamination Caused by TEPCO's Fukushima Daiichi
740 Nuclear Plant Accident. In: Takahashi, S. (Ed.), Radiation Monitoring and Dose
741 Estimation of the Fukushima Nuclear Accident. Spring, pp. 59-66. DOI:10.1007/978-4-
742 431-54583-5_6

743 Yoschenko, V., Takase, T., Konoplev, A., Nanba, K., Onda, Y., Kivva, S., Zheleznyak, M.,
744 Sato, N., Keitoku, K., 2017. Radiocesium distribution and fluxes in the typical
745 Cryptomeria japonica forest at the late stage after the accident at Fukushima Dai-Ichi
746 Nuclear Power Plant. J. Environ. Radioact. 166, 45-55.
747 DOI:10.1016/j.jenvrad.2016.02.017

748 **Figure Captions**

749 Figure 1. Relaxation mass depths obtained from fitting the profiles for the vertical distribution
750 of ^{137}Cs within soil at forests surveyed by the University of Tsukuba.

751 Figure 2. Schematic of the simulation model used for forests. Heights h_{T} and h_{LLB} represent
752 stand density weighted mean tree heights and lowest live branch heights, respectively. Details
753 of the organic layer and soil layers are shown in the enlarged region. Colors of layers match
754 those used in Figs. 5–7.

755 Figure 3. Convergence of estimates for uncertainties in simulated $\dot{H}^{*}(10)$ at 1 m height when
756 varying different input variables in their uncertainties distribution. Data is for site OT-S in 2016.
757 Black line showing total simulation uncertainty was calculated by varying all input variables
758 randomly in their uncertainty distributions.

759 Figure 4. Scatter plots showing correlation between measured and simulated $\dot{H}^{*}(10)$ in the
760 forests at (a) 0.1 m and (b) 1 m heights above the ground surface. As guides solid lines indicate
761 equality and dashed lines a factor of two deviation from equality are shown. Horizontal errors
762 bars show ± one standard error of $\dot{H}^{*}(10)$ measurements. Vertical errors show ± one standard
763 deviation of the calculated $\dot{H}^{*}(10)$ from simulations varying all input variables in the Gaussian
764 measurement uncertainty distributions.

765 Figure 5. Break down of contributions to $\dot{H}^{*}(10)$ at 1 m height from the simulation analysis.

766 Figure 6. Changes in distribution of ^{134}Cs and ^{137}Cs between the forest layers over time.

767 Figure 7. As per Figure 4, but results for $\dot{H}^{*}(10)$ at 20 m above the ground.

768 Figure 8. Graphs showing relative measurement uncertainties in model inputs (solid dots, left
769 vertical axis) and the consequent relative uncertainties in simulation outputs ($\dot{H}^{*}(10)$ at 1 m
770 height – bar plots, right vertical axis) for sites OT-Q, OT-S and TB-H, for 2011 and 2016.
771 Different classes of input variables are grouped per the labels on the horizontal axis. For classes
772 associated with more than one input variable (e.g. ^{134}Cs and ^{137}Cs radioactivities of the three

773 soil layers between 5 and 20 cm depth), the vertical line shows the range of uncertainties in the
774 inputs and the solid dot indicates the mean value.

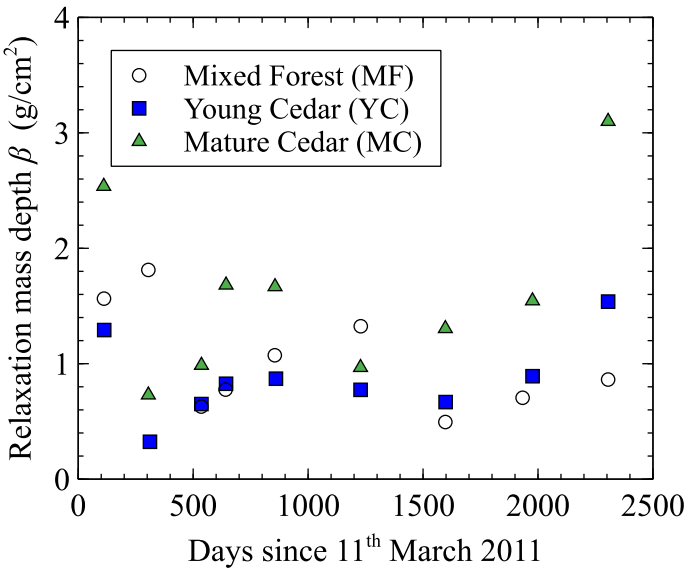

775

776 Figure 1

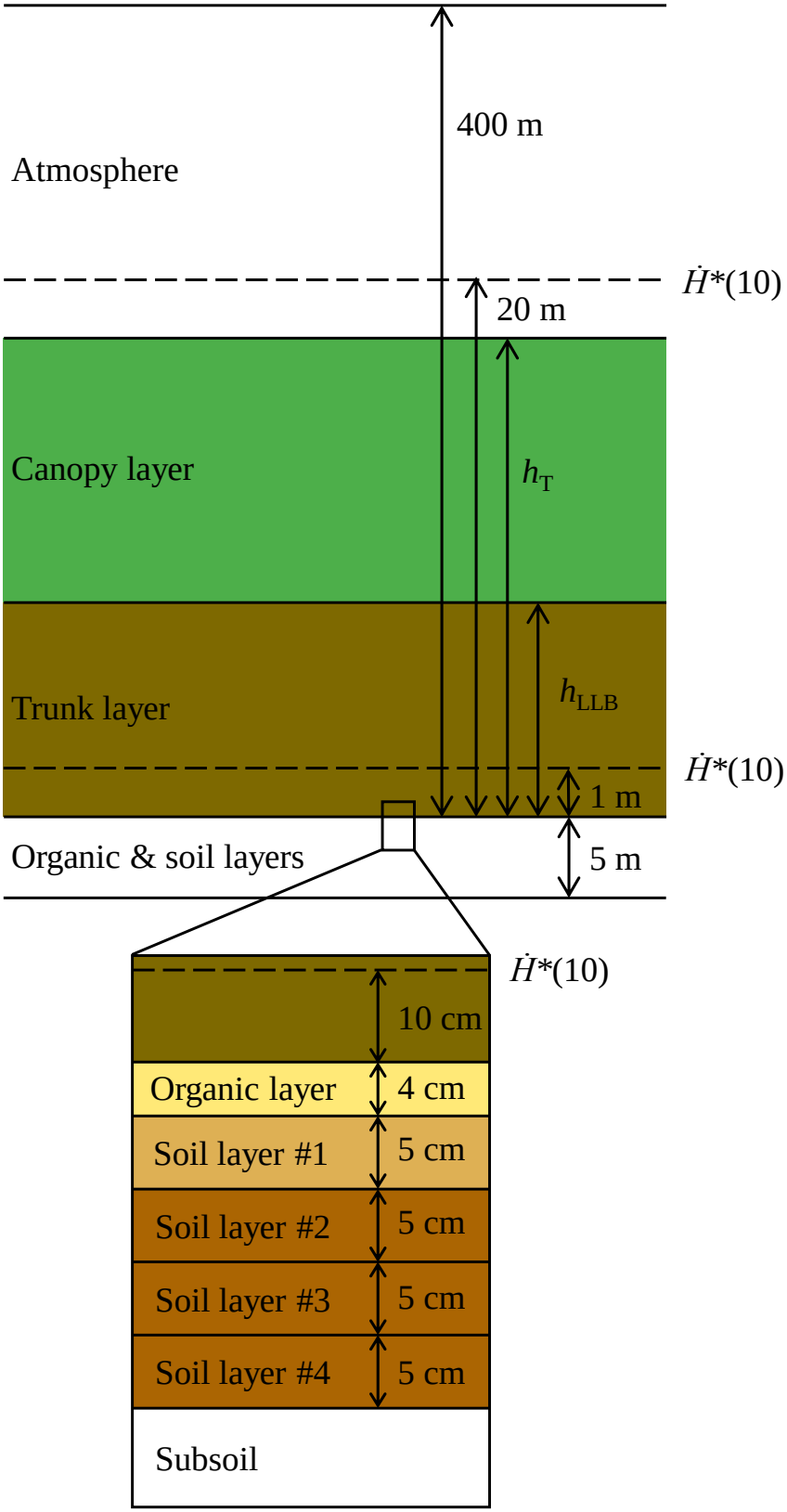

777

778 Figure 2

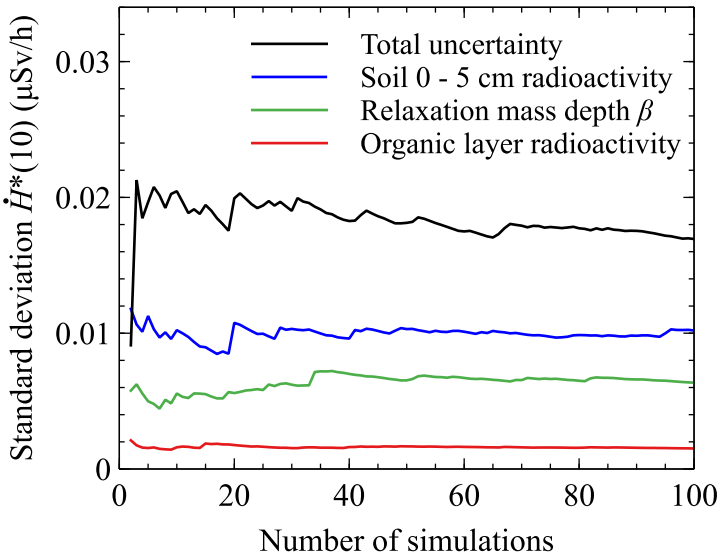

779

780 Figure 3

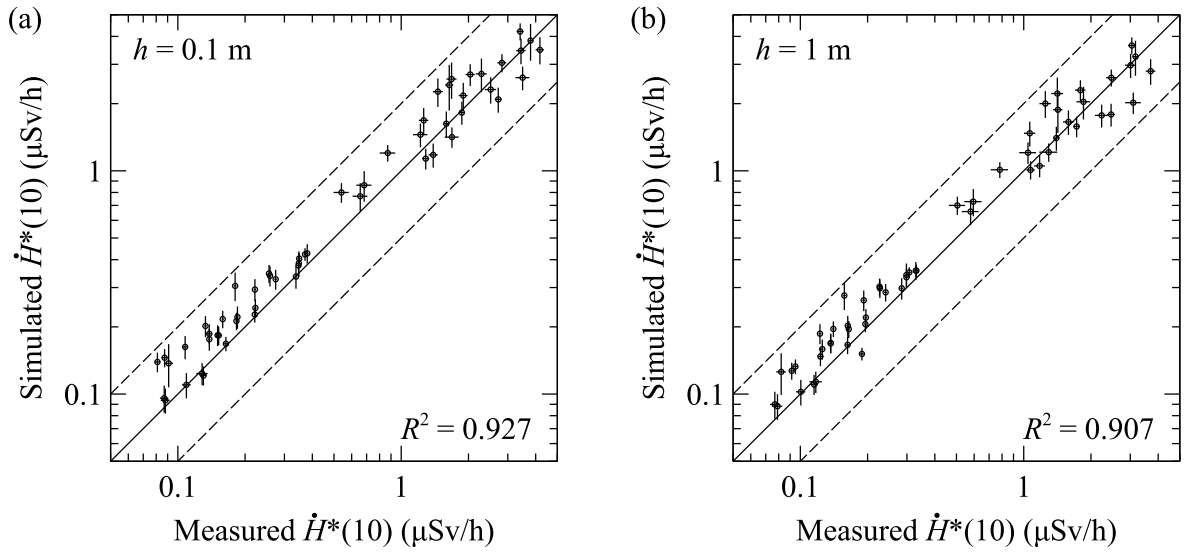

781

782 Figure 4

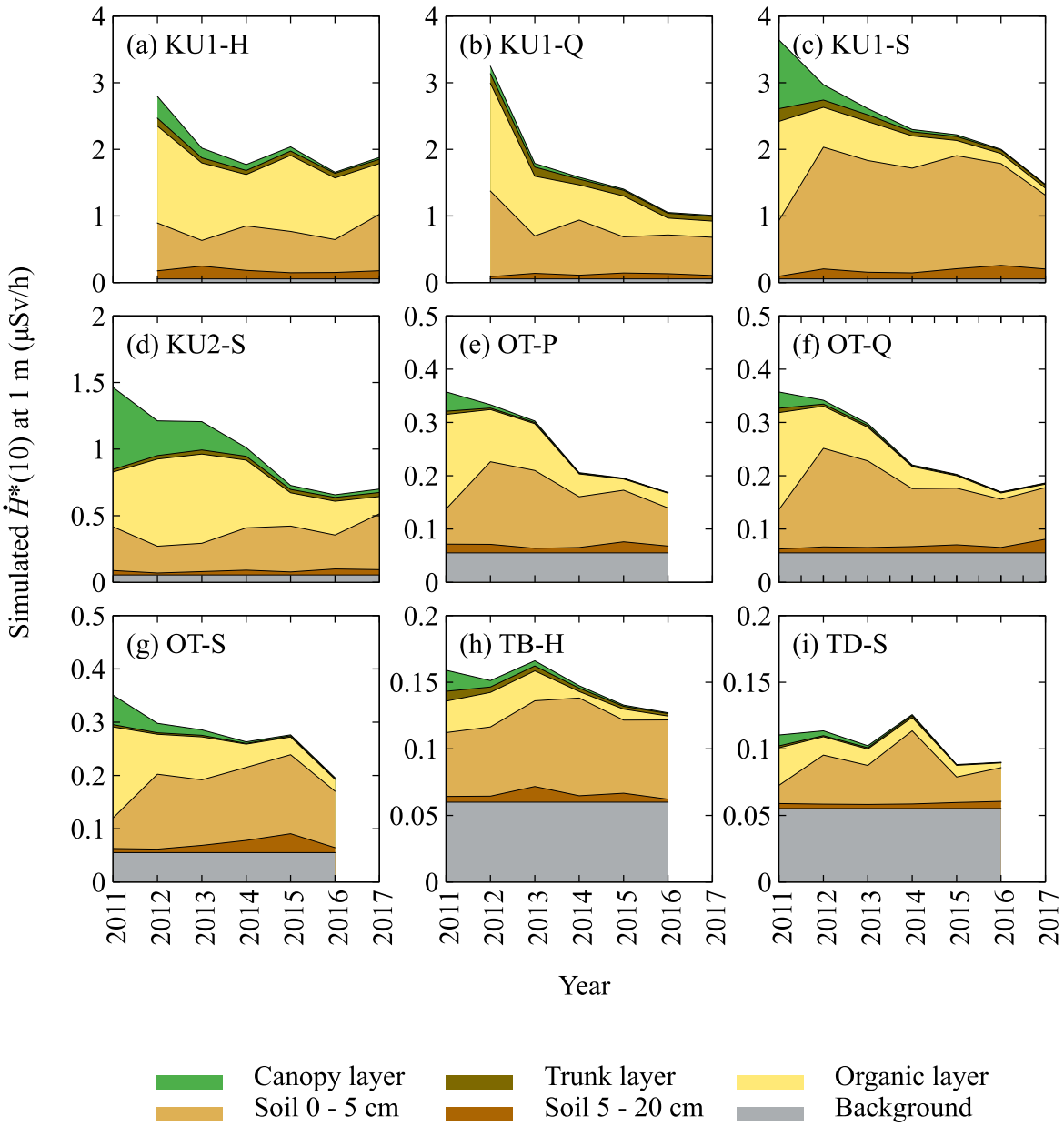

783

784

785 Figure 5

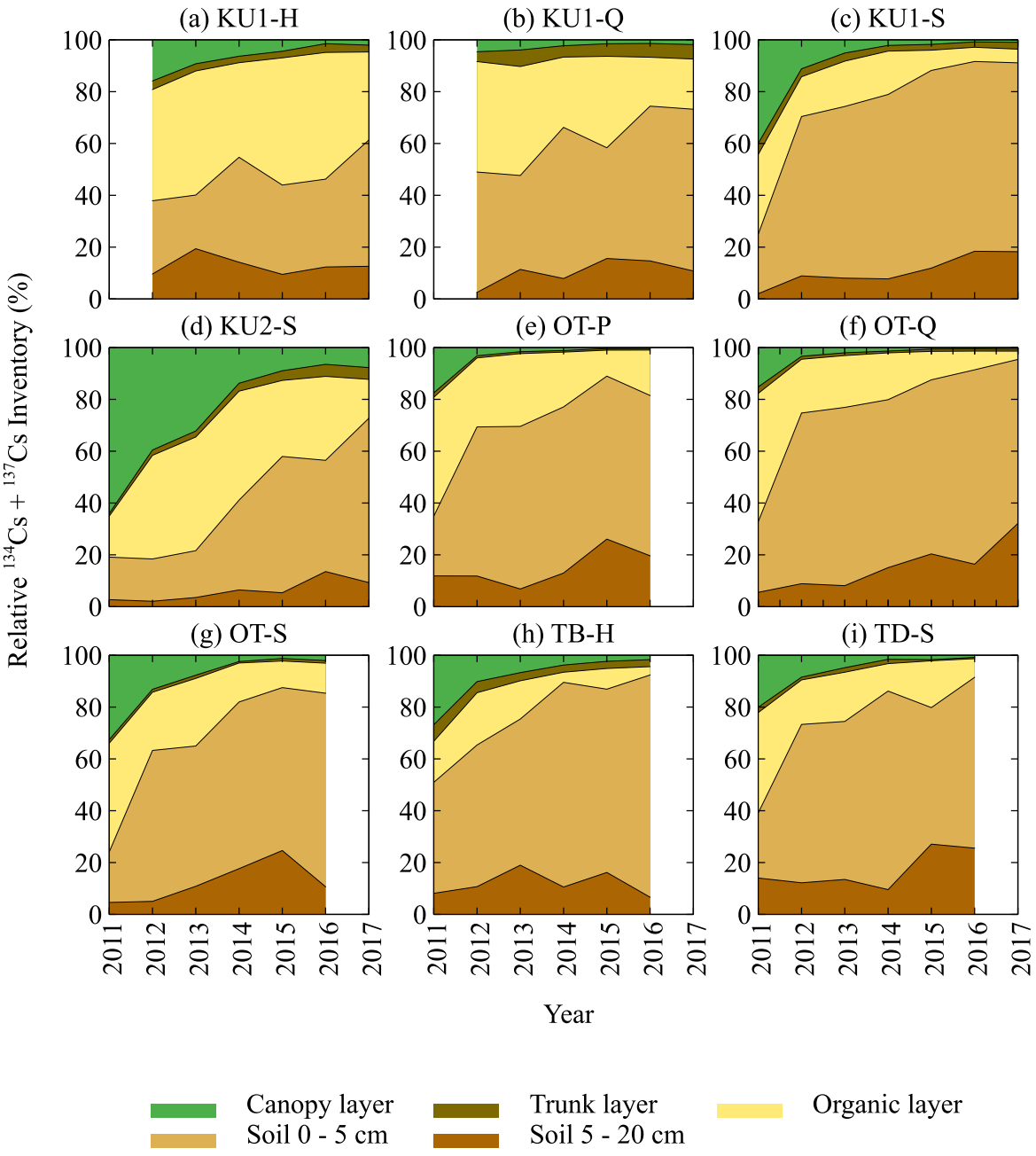

786

787

788 Figure 6

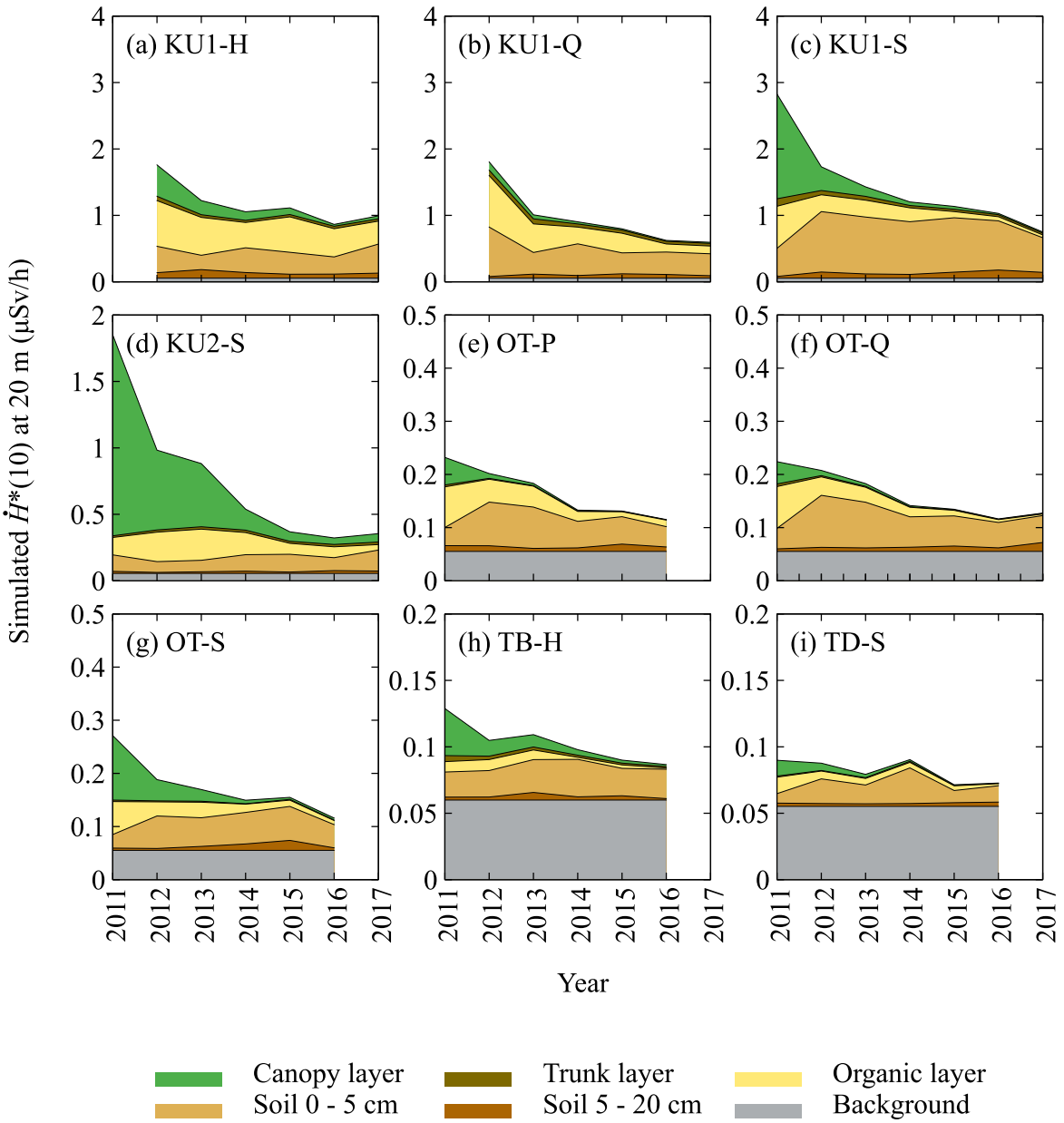

789

790

791 Figure 7

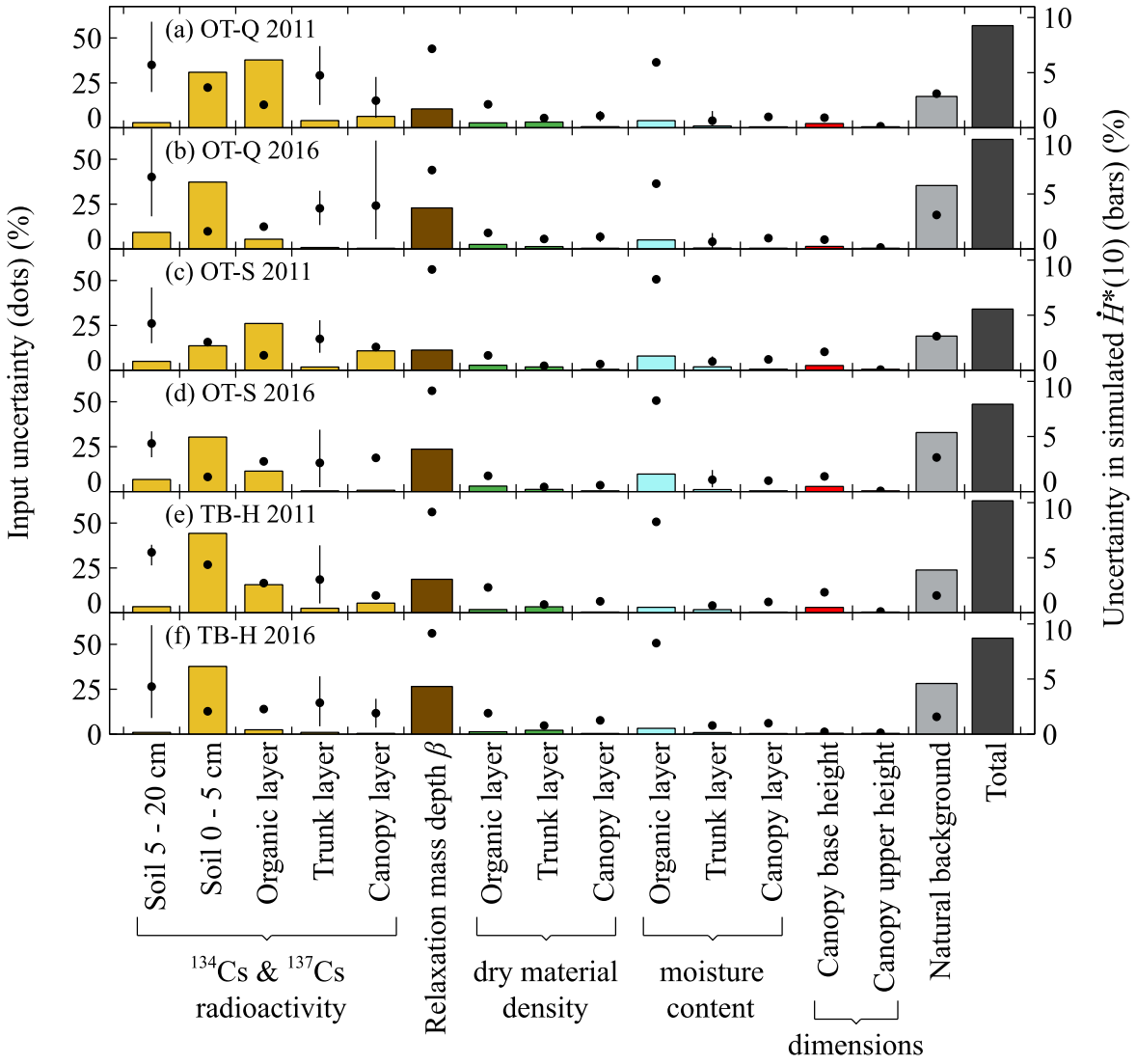

792

793 Figure 8

794 Table 1. Details of the nine FFPRI forest sites that were modelled. Mean stand densities are

795 averages over full survey periods.

Site code	Distance from FDNPP (km)	Tree species groups	Mean stand density (ha^{-1})	Survey period
KU1-H	27	Japanese cypress	1330	2012–17
KU1-Q	27	Konara oak and other broadleaf	1733	2012–17
KU1-S	26	Japanese cedar / mixed broadleaf	954 / 506	2011–17
KU2-S	28	Japanese cedar / Japanese larch / mixed broadleaf	725 / 199 / 33	2011–17
OT-P	66	Japanese red pine / mixed broadleaf	853 / 370	2011–16
OT-Q	66	Konara oak and other broadleaf / Japanese red pine	543 / 563	2011–17
OT-S	66	Japanese cedar	1117	2011–16
TB-H	160	Japanese cypress	2063	2011–16
TD-S	134	Japanese cedar / mixed broadleaf	1090 / 132	2011–16

796 Table 2. Elemental compositions of component materials used to make up simulation layers.

	Elemental composition (wt%)	Notes
Air	H, 0.064; C, 0.014; N, 75.1; O, 23.6; Ar, 1.28	Bellamy et al. (2018), volumetric density 1.2 kg/m^3
Dry organic matter (trunk and canopy layers)	H, 6.04; C, 50.4; N, 0.302; O, 43.3	Haraguchi et al. (1985) and Fukushima (2010)
Dry organic matter (organic & soil layers)	H, 6.05; C, 43.2; N, 2.72; O, 48.0	Mix cellulose and nitrogen, C/N mass ratio 15.9 (Kawada, 1982; 1989)
Dry black forest soil (andosol)	O, 46.3; Mg, 1.69; Al, 12.6; Si, 23.7; Ca, 2.43; Ti, 0.979; Fe, 10.7	AIST (2018)
Water (moisture)	H, 11.2; O, 88.8	Volumetric density 1000 kg/m^3

797

798 Table 3. Mean physical data over all survey years for each site. Note masses per unit area
799 include the moisture contents of the layer. For the canopy and trunk layers, they also include
800 the air mass (volumetric density 1.2 kg/m^3).

Site	Canopy base height (m)	Tree height (m)	Mass per unit area (kg/m^2)						
			Canopy layer	Trunk layer	Organic layer	Soil 0–5 cm	Soil 5–10 cm	Soil 10–15 cm	Soil 15–20 cm
KU1-S	6.7	14.2	15.4	36.6	2.9	29.1	38.4	42.0	44.8
KU1-H	4.0	16.9	21.0	32.7	2.8	31.1	39.4	41.6	40.7
KU1-Q	5.6	10.2	8.3	19.1	2.4	31.9	37.3	41.1	45.8
KU2-S	11.0	17.9	21.4	65.7	5.0	21.3	29.3	36.4	37.1
OT-S	11.9	18.1	16.8	54.7	3.6	25.4	31.5	33.3	34.3
OT-Q	7.4	12.1	10.8	29.4	2.8	29.0	37.0	40.3	42.6
OT-P	7.8	12.2	9.7	31.1	3.2	30.7	37.8	39.6	41.0
TD-S	7.7	14.3	14.6	36.8	2.8	32.7	41.7	52.2	55.0
TB-H	10.8	17.7	20.8	67.6	2.4	33.7	43.6	42.4	40.1
Max.	11.9	18.1	21.4	67.6	5.0	33.7	43.6	52.2	55.0
Min.	4.0	10.2	8.3	19.1	2.4	21.3	29.3	33.3	34.3

801 Table 4. Correspondence between simulated and measured $\dot{H}^*(10)$.

Metric	Height above ground	
	0.1 m	1 m
Root mean square deviation (μSv/h)	0.323	0.303
Mean percentage deviation (%)	18.9	15.7
Mean absolute percentage deviation (%)	23.6	21.6
Person correlation coefficient	0.963	0.952

802

Supplementary Information to Calculations for ambient dose equivalent rates in nine forests in eastern Japan from ^{134}Cs and ^{137}Cs radioactivity measurements

Table S1. Data sources for lower prevalence stand groups at sites with multiple stand groups.

Site	Tree species groups			Data for lower prevalence groups		Survey
	Main group	Secondary group	Tertiary group	Secondary group	Tertiary group	period
KU1-S	Japanese cedar	Mixed broadleaf	-	KU1-Q	-	2011–17
KU2-S	Japanese cedar	Japanese larch	Mixed broadleaf	OT-P	OT-Q	2011–17
OT-P	Japanese red pine	Mixed broadleaf	-	OT-Q	-	2011–16
OT-Q	Konara oak and other broadleaf	Japanese red pine	-	OT-P	-	2011–17
TD-S	Japanese cedar	Mixed broadleaf	-	OT-Q	-	2011–16

Table S2. Data from fits to ^{137}Cs vertical distributions within soil.

Survey	Mixed Forest (MF)				Young Cedar (MC)				Mature Cedar (MC)			
	Date	β (g/cm^2)	I_{inv} (Bq/cm^2)	Fit R^2	Date	β (g/cm^2)	I_{inv} (Bq/cm^2)	Fit R^2	Date	β (g/cm^2)	I_{inv} (Bq/cm^2)	Fit R^2
1	1-Jul-11	1.56	3.7	0.983	2-Jul-11	1.29	2.7	0.992	30-Jun-11	2.54	26.0	0.975
2	10-Jan-12	1.81	15.9	0.997	17-Jan-12	0.32	4.3	0.962	10-Jan-12	0.73	15.7	0.997
3	27-Aug-12	0.63	12.4	0.951	28-Aug-12	0.65	12.0	0.964	28-Aug-12	0.99	45.0	0.923
4	11-Dec-12	0.78	23.4	0.970	13-Dec-12	0.83	21.6	0.994	13-Dec-12	1.68	21.2	0.934
5	13-Jul-13	1.07	10.0	0.993	18-Jul-13	0.87	10.3	0.957	14-Jul-13	1.67	26.3	0.999
6	22-Jul-14	1.32	20.0	0.996	21-Jul-14	0.77	30.3	0.974	21-Jul-14	0.97	39.5	0.995
7	25-Jul-15	0.49	28.1	0.996	26-Jul-15	0.67	23.9	0.999	25-Jul-15	1.30	45.4	0.996
8	25-Jun-16	0.70	22.5	0.996	7-Aug-16	0.89	31.9	0.999	7-Aug-16	1.54	49.6	0.999
9	2-Jul-17	0.86	25.3	0.992	2-Jul-17	1.54	34.1	0.995	2-Jul-17	3.10	55.0	0.993

Note: Moisture contents were available from surveys 2, 3, 7 and 9 for the Mixed Forest, and surveys 2, 3, 6, 7 and 9 for the Young Cedar and Mature Cedar forests, to convert masses of oven-dried soil layer samples to wet masses. This data was used directly for converting the masses for these surveys. For other surveys, mean moisture contents applicable for each forest were used instead.

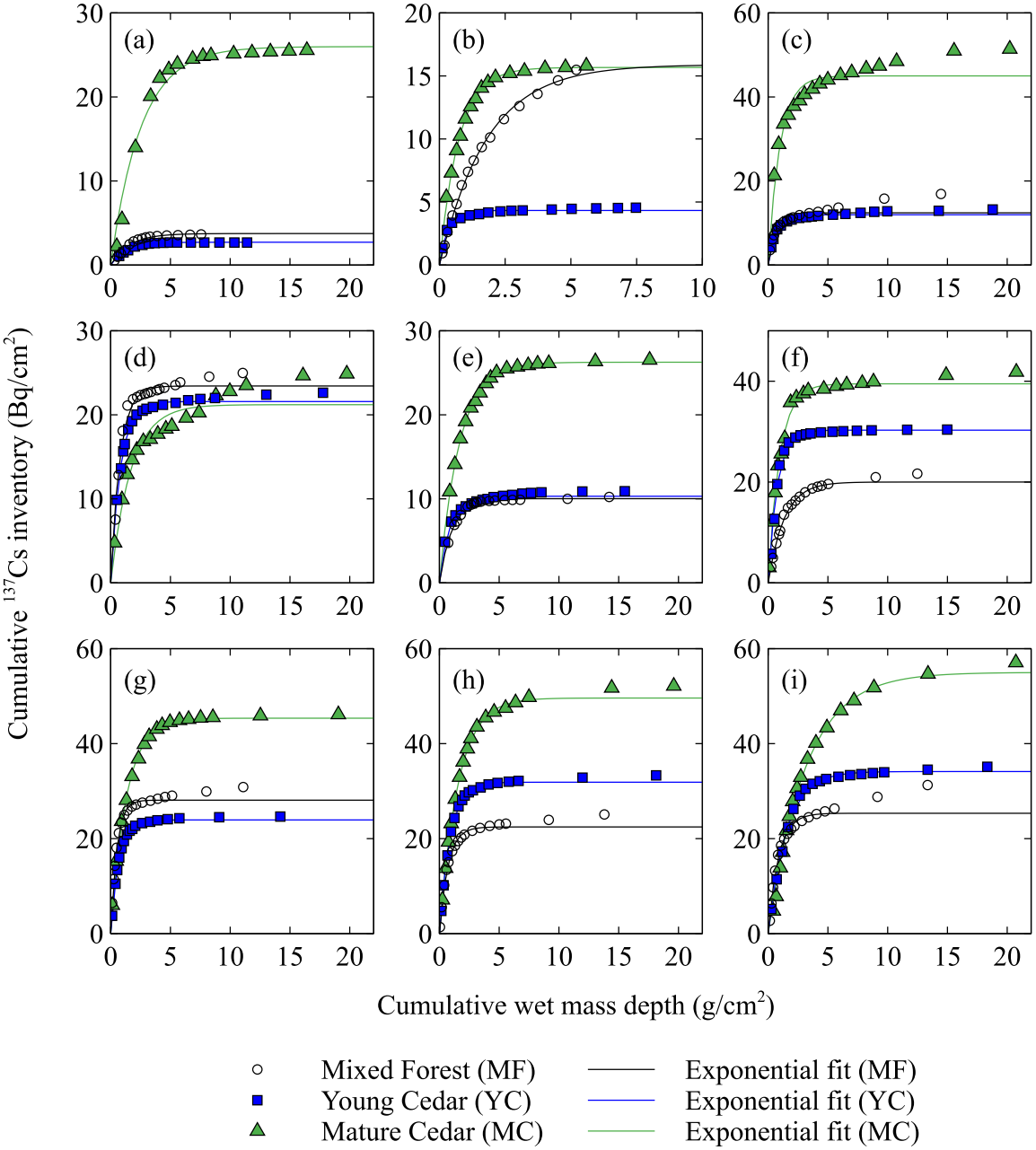

Figure S1. Fits of cumulative exponential distributions to cumulative distributions of ^{137}Cs with mass depth vertically in wet soil at the sites surveyed by the University of Tsukuba. Panels (a) to (i) show results over time from surveys 1 (in June 2011) to 9 (in June 2017)